A Multielectrode Electrochemical and Scanning Differential Electrochemical Mass Spectrometry Study of Methanol Oxidation on Electrodeposited Pt_xRu_y

K. Jambunathan,† S. Jayaraman, and A. C. Hillier*

Department of Chemical Engineering, Department of Chemistry, and Institute for Combinatorial Discovery, Iowa State University, Ames, Iowa 50011

Received August 25, 2003. In Final Form: December 11, 2003

Methanol electro-oxidation was studied on a series of electrodeposited Pt_xRu_y catalysts constructed as multielement band electrodes. A combination of electrochemical and scanning differential electrochemical mass spectrometry measurements were performed to evaluate the composition-dependence of methanol oxidation, methanol decomposition, CO_2 current efficiency, and the product distribution at 25 and 50 °C. At 25 °C, cyclic voltammetry revealed that the presence of Ru led to enhanced methanol oxidation rates over that of pure Pt. Methanol decomposition showed a similar composition-dependence. Mass spectrometry measurements revealed the evolution of HCOOH and CO_2 during methanol oxidation and allowed indirect determination of H_2CO produced. Notably, these products were not observed during methanol decomposition. The most active electrode compositions and the highest instantaneous current efficiencies for the formation of CO_2 were found to depend on several factors. At 25 °C, the maximum activity was ∼10% Ru, while at 50 °C the most active composition increased to ∼25% Ru. Pure Pt had the highest instantaneous current efficiency for CO_2 at both temperatures. The product distribution reflected high CO_2 evolution for Pt, with an increasing fraction of the product emerging as H_2CO at higher Ru content. Increasing the temperature improved the CO_2 current efficiency for all electrode compositions. These results confirm that methanol oxidation occurs though a parallel reaction pathway on Pt_xRu_y electrodes. In addition, the balance between the different reaction pathways depends on several factors, including Ru composition and temperature.

Introduction

Methanol oxidation is a reaction of technological interest because of its potential application as a fuel in low-temperature fuel cells.[1−4] However, methanol presents considerable performance challenges, including substantial catalyst poisoning at the anode and significant membrane crossover that reduces cathode activity. The overall electrochemical reaction for methanol oxidation involves the transfer of six electrons.

$$CH_3OH + H_2O \rightarrow CO_2 + 6H^+ + 6e^- \qquad (1)$$
$$E^0 = 0.03 \text{ V vs RHE}$$

However, the true reaction pathway is much more complex. Numerous studies have established that methanol oxidation on platinum involves the formation of partial oxidation products[5−8] through a competing, parallel path mechanism.[7,9,10] Both strongly adsorbed surface species such as carbon monoxide and weakly bound reactive intermediates such as formic acid and formaldehyde[5,11,12] have been observed during methanol oxidation in addition to carbon dioxide, which is the complete oxidation product. Ultimately, the complexity of this reaction and the formation of electrode-deactivating partial oxidation products limits the ability of many anode catalysts to carry out this reaction.

Considerable effort has been expended to develop catalysts with higher poison tolerance and greater methanol oxidation activity.[13−15] Platinum is the only single-component catalyst that shows a significant activity for methanol oxidation at ambient temperature. However, this activity is too low to be considered practical for commercial fuel cells. Improved activity has been observed in multicomponent catalysts that include components such as Ru,[16−18] Sn,[19−21] Mo,[22−24] and Os.[25] These components represent oxophilic metals that promote water decom-

* To whom correspondence should be addressed. E-mail: hillier@iastate.edu.

† Current address: Department of Chemistry, Pennsylvania State University, University Park, PA 16802.

(1) Wasmus, S.; Kuver, A. *J. Electroanal. Chem.* **1999**, *461*, 14.
(2) Jarvi, T. D.; Stuve, E. M. In *Electrocatalysts*; Ross, P. N., Lipkowski, J., Eds.; Wiley: New York, 1998.
(3) Iwasita, T. *Electrochim. Acta* **2002**, *47*, 3663.
(4) Lamy, C.; Lima, A.; LeRhun, V.; Delime, F.; Coutanceau, C.; Leger, J. M. *J. Power Sources* **2002**, *105*, 283.
(5) Belgsir, E. M.; Huser, H.; Leger, J.-M.; Lamy, C. *J. Electroanal. Chem* **1987**, *225*, 281.
(6) Wasmus, S.; Wang, J. T.; Savinell, R. F. *J. Electrochem. Soc* **1995**, *142*, 3825.
(7) Sriramulu, S.; Jarvi, T. D.; Stuve, E. M. *Electrochim. Acta* **1998**, *44*, 1127.
(8) Wang, H.; Loffler, T.; Baltruschat, H. *J. Appl. Electrochem.* **2001**, *31*, 759.
(9) Jarvi, T. D.; Sriramulu, S.; Stuve, E. M. *Colloid Surf., A* **1998**, *134*, 145.
(10) Sriramulu, S.; Jarvi, T. D.; Stuve, E. M. *J. Electroanal. Chem.* **1999**, *467*, 132.
(11) Korzeniewski, C.; Childers, C. L. *J. Phys. Chem. B* **1998**, *102*, 489.
(12) Childers, C. L.; Huang, H.; Korzeniewski, C. *Langmuir* **1999**, *15*, 786.
(13) Anderson, A. B.; Grantscharova, E.; Seong, S. *J. Electrochem. Soc.* **1996**, *143*, 2075.
(14) Gurau, B.; Viswanathan, R.; Liu, R. X.; Lafrenz, T. J.; Ley, K. L.; Smotkin, E. S.; Reddington, E.; Sapienza, A.; Chan, B. C.; Mallouk, T. E.; Sarangapani, S. *J. Phys. Chem. B* **1998**, *102*, 9997.
(15) Kua, J.; Goddard, W. A. *J. Am. Chem. Soc.* **1999**, *121*, 10928.
(16) Watanabe, M.; Motoo, S. *J. Electroanal. Chem. Interfacial Electrochem.* **1975**, *60*, 267.
(17) Gasteiger, H. A.; Markovic, N.; Ross, P. N.; Cairns, E. J. *J. Phys. Chem.* **1993**, *97*, 12020.
(18) Chrzanowski, W.; Wieckowski, A. *Langmuir* **1998**, *14*, 1967.
(19) Janssen, M. M. P.; Moolhuysen, J. *J. Catal.* **1977**, *46*, 289.
(20) Wang, K.; Gasteiger, H. A.; Markovic, N. M.; Ross, P. N. *Electrochim. Acta* **1996**, *41*, 2587.
(21) Morimoto, Y.; Yeager, E. B. *J. Electroanal. Chem.* **1998**, *444*, 95.
(22) Kita, H.; Nakajima, H.; Shimazu, K. *J. Electroanal. Chem.* **1988**, *248*, 181.
(23) Nakajima, H.; Kita, H. *Electrochim. Acta* **1990**, *35*, 849.
(24) Wang, Y.; Fachini, E. R.; Cruz, G.; Zhu, Y.; Ishikawa, Y.; Colucci, J. A.; Cabrera, C. R. *J. Electrochem. Soc* **2001**, *148*, C222.
(25) Crown, A.; Moraes, I. R.; Wieckowski, A. *J. Electroanal. Chem.* **2001**, *500*, 333.

10.1021/la035567i CCC: $27.50
Published on Web 01/29/2004

position and form surface oxides or hydroxides at low potentials, which can assist in oxidizing adsorbed intermediates such as CO on neighboring platinum sites.[14] Additional improvements have been seen with ternary[26−28] and quaternary systems,[14,29−31] where enhanced activity is attributed to facilitated water activation and increased C−H bond-breaking ability in these multicomponent catalysts.[14] Ultimately, the discovery of improved catalysts for methanol oxidation will require a thorough exploration of the vast composition space available for catalyst construction. The application of combinatorial techniques poses considerable promise in accelerating the discovery of novel catalyst materials.[14,29,31−33]

We recently described a tool for combinatorial electrochemical studies called the scanning differential electrochemical mass spectrometer (SDEMS).[34] This technique combines the attributes of differential electrochemical mass spectrometry (DEMS) with a scanning inlet probe. DEMS has been used extensively to study the formation of volatile products during electrode reactions, including methanol oxidation at porous electrodes, nanoparticle catalysts, and solid electrode surfaces.[35−41] This technique is particularly useful in measuring the distribution of the various partial and complete oxidation products as well as establishing the efficiency of the complete oxidation reaction for fuels such as methanol, ethanol, and formic acid.[42,43] Recent applications of a capillary-flow DEMS system have examined the kinetics of hydrogen oxidation, carbon monoxide oxidation,[44] and methanol oxidation[45] on unsupported platinum and platinum−ruthenium catalysts.[46]

In this work, we employ multielectrode electrochemical measurements in concert with SDEMS to interrogate the composition-dependence of a catalyst library consisting of electrodeposited Pt_xRu_y band electrodes. We examine methanol oxidation, methanol decomposition, CO_2 current efficiency, and the product distribution at ambient and elevated temperatures on a series of Pt_xRu_y electrodes with varying composition within the same experimental cell. The activity trends are consistent with those of previous catalyst studies while also providing information about reaction efficiencies and product distribution trends at two different temperatures. The simultaneous evaluation of multiple electrodes with differing composition allows a direct comparison of activities under identical operating conditions. This also represents a convenient experimental platform for catalyst screening and detailed analysis of reaction pathways and reaction efficiencies.

Experimental Section

Materials. *Reagents.* All experiments were performed using electrolytes in 18 MΩ deionized water (E-Pure, Barnstead, Dubuque, IA). The solutions were deaerated by bubbling with nitrogen (BOC Gases, Murray Hill, NJ) prior to each measurement. Electrolyte solutions contained sulfuric acid (H_2SO_4) and methanol (CH_3OH, 99.9%) (Aldrich, Milwaukee, WI), which were used as received. Electrodeposits of Pt and Ru were fabricated from solutions containing chloroplatinic acid (H_2PtCl_6, Strem Chemicals, Newburyport, MA) and ruthenium chloride ($RuCl_3$, Strem Chemicals, Newburyport, MA).

Electrodes. Working electrodes consisted of Pt_xRu_y catalysts of varying composition that were electrochemically deposited onto Au band electrodes. The band electrodes were prepared by vapor-depositing Au through a mask onto the surface of a roughened glass slide (Erie Scientific, Portsmouth, NH) followed by electrodeposition. The roughened glass was used to enhance gold adhesion and to create a higher surface area electrode. A mask containing eight slits ($^1/_{32}$ in. wide and $^1/_{16}$ in. spacing) made of aluminum was used to create the electrodes on the roughened glass slide. A 100 nm gold (Ernest F. Fullam Inc., Latham, NY) layer was evaporated onto the glass slide though the Al mask using a thermal vacuum evaporator (Model Bench Top Turbo III, Denton Vacuum, Moorestown, NJ), which created gold band electrodes that were electrically separated from each other. Pt and Ru were coelectrodeposited onto the gold electrodes from 0.1 M Na_2SO_4 solutions containing different amounts of H_2PtCl_6 and $RuCl_3$. The deposition procedure utilized a pulsed potential program that applied a square wave to the band electrodes with potential limits of 0.5 and −1.0 V vs RHE at a frequency of 100 Hz with a potentiostat (model 283, EG&G Instruments, Oakridge, TN) and a function generator (Global Specialities, New Haven, CT). A Pt−Ir coated Ti mesh was used as counter electrode and a $Hg|Hg_2SO_4$ electrode was used for the reference. Electrodeposition was carried out by injecting a solution of known metal composition into the electrochemical cell and applying the potential waveform to one of the eight electrode bands for a period of 5 min. Following deposition, the cell was thoroughly rinsed with deionized water before a new solution composition was injected. Electrodeposition was completed in a serial fashion until all electrodes were coated. For the Pt_xRu_y electrodes, the deposition solutions for the eight bands consisted of Pt/Ru solution with molar ratios of 100/0, 90/10, 70/30, 40/60, 60/40, 30/70, 10/90, and 0/100. Four identical samples were prepared and tested with a combination of scanning differential electrochemical mass spectrometry (SDEMS), Auger electron spectroscopy (AES), scanning electron microscopy (SEM), energy-dispersive X-ray spectroscopy (EDS), and cyclic voltammetry.

Methods. *Electrochemistry.* Cyclic voltammetry was performed on the substrate electrodes using a multielectrode potentiostat (model CH1030, CH Instruments Inc., Austin, TX), which could control eight working electrodes simultaneously. The working electrode leads were connected to eight of the pins of a 20-pin dip-clip (Pomona Electronics, Pomona, CA), which was attached to the substrate electrode. A wound Pt−Ir counter electrode and a $Hg|HgSO_4$ reference electrode were used during voltammetry experiments. The electrochemical cell consisted of a 1 in. × 0.5 in. × 1 in. rectangular glass tube (Whale Apparatus Company, Inc., Hellertown, PA) that was glued directly to the band electrode assembly using a stop-off coating (WB-018, Michigan Chrome and Chemical Company, Hope, AK). For high-temperature experiments, heating was achieved using a flexible strip heater (Omega, Stamford, CT) wrapped around the glass tube. The temperature was controlled using a benchtop temperature controller (model CS3910, Omega, Stamford, CT) with a Teflon coated thermocouple probe.

(26) Lima, A.; Coutanceau, C.; Leger, J. M.; Lamy, C. *J. Appl. Electrochem.* **2001**, *31*, 379.
(27) Jusys, Z.; Schmidt, T. J.; Dubau, L.; Lasch, K.; Jorissen, L.; Garche, J.; Behm, R. J. *J. Power Sources* **2002**, *105*, 297.
(28) Ley, K. L.; Liu, R. X.; Pu, C.; Fan, Q. B.; Leyarovska, N.; Segre, C.; Smotkin, E. S. *J. Electrochem. Soc.* **1997**, *144*, 1543.
(29) Reddington, E.; Sapienza, A.; Gurau, B.; Viswanathan, R.; Sarangapani, S.; Smotkin, E. S.; Mallouk, T. E. *Science* **1998**, *280*, 1735.
(30) Arico, A. S.; Creti, P.; Giordano, N.; Antonucci, V.; Antonucci, P. L.; Chuvilin, A. *J. Appl. Electrochem.* **1996**, *26*, 959.
(31) Choi, W. C.; Kim, J. D.; Woo, S. I. *Catal. Today* **2002**, *74*, 235.
(32) Liu, R. X.; Smotkin, E. S. *J. Electroanal. Chem.* **2002**, *535*, 49.
(33) Nayar, A.; Liu, R.; Allen, R. J.; McCall, M. J.; Willis, R. R.; Smotkin, E. S. *Anal. Chem.* **2002**, *74*, 1933.
(34) Jambunathan, K.; Hillier, A. C. *J. Electrochem. Soc.* **2003**, *150*, E312.
(35) Wolter, O.; Heitbaum, J. *Ber. Bunsen-Ges. Phys. Chem.* **1984**, *88*, 2.
(36) Willsau, J.; Wolter, O.; Heitbaum, J. *J. Electroanal. Chem.* **1985**, *185*, 163.
(37) Willsau, J.; Heitbaum, J. *J. Electroanal. Chem.* **1985**, *185*, 181.
(38) Willsau, J.; Heitbaum, J. *Electrochim. Acta* **1986**, *31*, 943.
(39) Wilhelm, S.; Vielstich, W.; Buschmann, H. W.; Iwasita, T. *J. Electroanal. Chem.* **1987**, *229*, 377.
(40) Iwasita, T.; Vielstich, W.; Santos, E. *J. Electroanal. Chem.* **1987**, *229*, 367.
(41) Buschmann, H. W.; Wilhelm, S.; Vielstich, W. *Electrochim. Acta* **1986**, *31*, 939.
(42) Jusys, Z.; Kaiser, J.; Behm, R. J. *Langmuir* **2003**, *19*, 6759.
(43) Wang, H.; Wingender, C.; Baltruschat, H.; Lopez, M.; Reetz, M. T. *J. Electroanal. Chem.* **2001**, *509*, 163.
(44) Jusys, Z.; Massong, H.; Baltruschat, H. *J. Electrochem. Soc.* **1999**, *146*, 1093.
(45) Jusys, Z.; Behm, R. J. *J. Phys. Chem. B* **2001**, *105*, 10874.
(46) Jusys, Z.; Kaiser, J.; Behm, R. J. *Electrochim. Acta* **2002**, *47*, 3693.

Scheme 1. Schematic of Eight-Element Band Electrodes with Electrodeposited Pt_xRu_y Catalyst Samples[a]

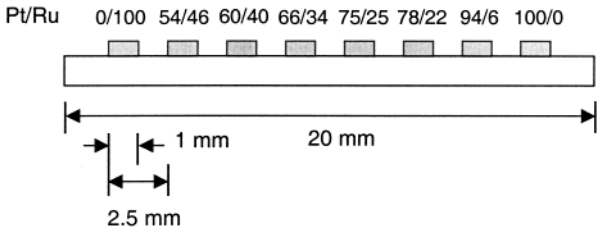

[a] The electrode compositions are given in percentages as determined by Auger electron spectroscopy.

Scanning Differential Electrochemical Mass Spectrometry (SDEMS). The configuration and performance of the SDEMS system used in this work has been described in detail.[34] Briefly, the SDEMS consisted of an electrochemical cell and potentiostat combined with a mass spectrometer and three-dimensional positioning system, which were all under computer control. The mass spectrometer (MS) was a QMS 200 (Pfeiffer Vacuum, Nashua, NH). The spectrometer utilized an electron impact (EI) ionization source, and pumping of the detector's ionization chamber was achieved with a combination of mechanical diaphragm roughing pump and a turbomolecular pump. The inlet to the MS consisted of a 150 μm diameter (i.d.) PTFE capillary tube (Valco Instruments, Houston, TX) to which a 20 nm pore size Gore-Tex membrane was secured with heat-shrink tubing. The capillary sampling probe was mounted to a holder attached to a three-dimensional piezoelectric-driven positioning system (Burleigh Instruments, Inc., Fishers, NY). Electrochemical measurements were performed using a bipotentiostat (AFDRE, Pine Instrument Company, Grove City, PA). Data collection was achieved using a commercial mass spectrometer controller program (Quadstar, Balzers Limited, FL).

Scanning Electron Microscopy. Surface topography and bulk compositional analysis of the Pt_xRu_y band electrodes were performed using a JEOL JXA 840A scanning electron microscope equipped with an X-ray detector (Princeton Gamma-Tech Inc., Princeton, NJ) for energy dispersive spectroscopy (EDS) analysis. An accelerating voltage of 20 kV was used in all SEM experiments. Double-sided copper adhesive tape (3M Electrical Products Division, Austin, TX) was used to provide electrical contact between the substrate and the sample mount in order to prevent the charging effects during SEM measurements. The Pt Mα peak at 2.050 keV and the Ru Lα peak at 2.558 keV were used to determine the bulk compositions of the band electrodes.

Auger Electron Spectroscopy. Surface compositions of the Pt_x-Ru_y band electrode were verified using a model Φ560 Auger electron spectroscope (Physical Electronics, Eden Prairie, MN). An accelerating voltage of 3 kV was used in all AES measurements. Pt-MNN peak at 69 eV and Ru-MNN peak at 269 eV were used for the quantitative analysis of Pt and Ru. A double-sided copper adhesive tape was used to provide electrical contact between the substrate and the sample mount to minimize charging effects.

Results and Discussion

Catalysts of various Pt_xRu_y compositions were fabricated by pulsed potential, electrochemical deposition from solutions containing H_2PtCl_6 and $RuCl_3$ onto multielement band electrodes (Scheme 1). Deposition was typically performed for about 5 min until a dense, high-coverage layer of particles formed with diameters between 200 and 500 nm (Figure 1A). The Pt_xRu_y samples included eight compositions ranging from pure Pt to pure Ru as determined by AES (Figure 1B). EDS provided equivalent values for the various electrode compositions, which suggests that the bulk and surface compositions of these samples are similar.

Figure 2A depicts steady-state cyclic voltammetry measurements for the various Pt_xRu_y electrodes in a solution of 1.0 M CH_3OH in 0.5 M H_2SO_4 at 25 °C. For all electrodes, negligible current is observed at potentials below 0.3 V. This reflects minimal methanol oxidation in this potential range. The presence of adsorbed carbon monoxide, which forms as a result of methanol decom-

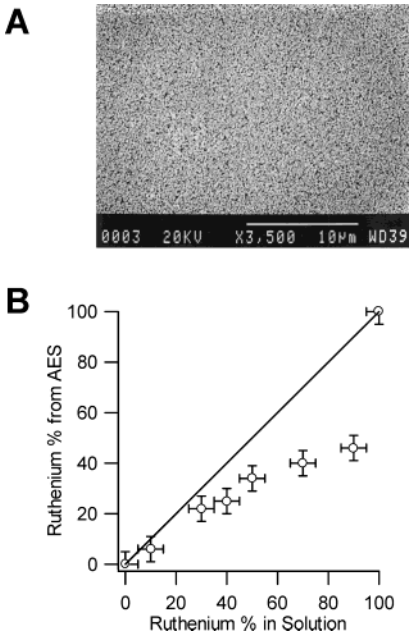

Figure 1. (A) Scanning electron micrograph of electrodeposited Pt electrode. (B) Compositions of electrodeposited Pt_xRu_y electrodes as determine by AES compared to solution ruthenium content.

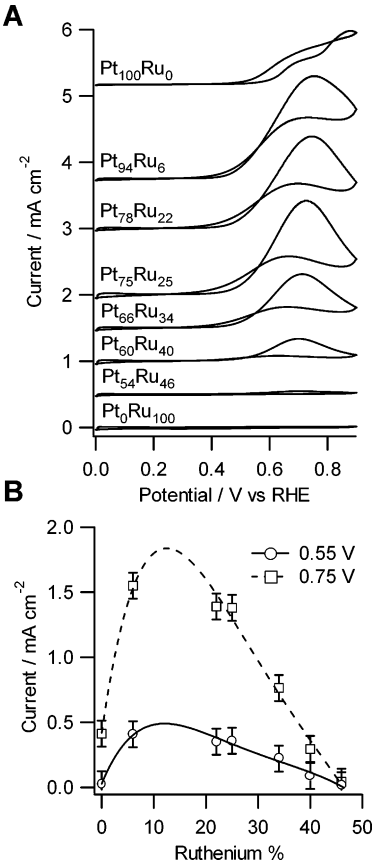

Figure 2. (A) Steady-state cyclic voltammetry of Pt_xRu_y electrodes in a 1.0 M CH_3OH and 0.5 M H_2SO_4 solution at 25 °C. Scan rate is 0.01 V s^{-1}. (B) Plot of current from (A) versus ruthenium composition at substrate potentials of 0.55 and 0.75 V.

position, prevents the adsorption of either hydrogen or methanol at these potentials. Increasing the electrode potential generates oxidation current with different onset potentials, peak potentials, and peak currents for the various electrodes. The pure platinum electrode ($Pt_{100}Ru_0$) starts generating oxidation current at ~0.5 V, and the magnitude increases with increasing electrode potential. In contrast, pure ruthenium (Pt_0Ru_{100}) exhibits little measurable methanol oxidation current over the entire potential range studied. The latter behavior reflects a very low intrinsic activity for methanol oxidation on ruthenium. This is related to the high barrier for methanol decomposition on ruthenium, which has been attributed to the blocking effect of adsorbed hydrogen at potentials below 0.2 V and surface oxides at potentials above 0.2 V.[47]

The electrodes possessing a mixture of platinum and ruthenium show a range of activities. The addition of Ru to the Pt electrode results in a decrease in the onset potential for methanol oxidation and an increase in the peak oxidation current. Figure 2A illustrates that the electrodes with Ru contents of 6, 22, 25, and 34% exhibit current onsets near 0.35 V, which is about 0.15 V lower than that observed for pure Pt. The methanol oxidation currents increase as the potential increases until a maximum is reached near 0.75 V. The maximum current densities exhibited by the $Pt_{94}Ru_6$ and $Pt_{78}Ru_{22}$ electrodes are roughly twice that of the $Pt_{100}Ru_0$ electrode. Increasing the Ru content beyond 34% decreases the oxidation current and increases the onset potential. The electrode containing 46% Ru behaves similarly to that of pure Ru with very limited activity.

A comparison of the oxidation currents for the various electrodes at potentials of 0.55 and 0.75 V during the anodic potential scan shows a composition-dependent activity with a clear maximum over a range of Ru content (Figure 2B). The electrode exhibiting the greatest current at both 0.55 and 0.75 V contains 6% Ru. The pure Pt electrode shows considerably lower activity. Although the 6% Ru electrode shows the highest measured activity, a smooth curve drawn through the data points suggests that the most active composition lies in a range between 5 and 25% Ru with a maximum of ~10%. These results are consistent with the idea that the Pt_xRu_y catalysts function through a "bifunctional mechanism" in which the ruthenium sites dissociate water to form hydroxide and promote the oxidation of CO on neighboring Pt sites.[14,16]

Further insight into the impact of electrode composition can be gained by examining methanol decomposition. Methanol decomposition can be directly investigated by cyclic voltammetry (Figure 3). In these measurements, the catalyst electrodes were placed in sulfuric acid solution and held at 0.05 V. Methanol at a concentration of 1.0 M was then introduced and the electrodes held for a period of 5 min. The electrode potential was then cycled down to 0.0 V before scanning in the positive direction. This procedure creates an initially hydrogen-covered electrode surface that is free of methanol until the potential is swept in the positive direction. Current measured during the positive sweep reflects a combination of hydrogen desorption and methanol adsorption/decomposition.

The pure Pt electrode shows very little current until a potential 0.1 V is reached in the positive-going scan. Below this potential, the Pt surface is covered with a layer of adsorbed hydrogen, which blocks sites required for methanol adsorption. Above 0.1 V, hydrogen desorbs and free Pt sites appear on which methanol adsorption and

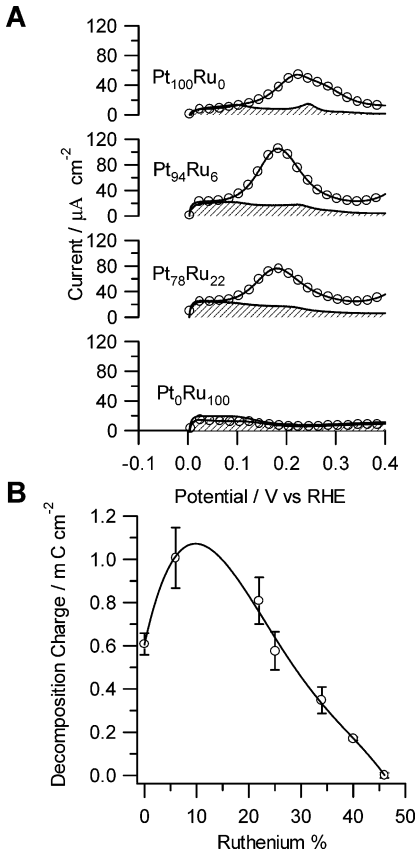

Figure 3. (A) Cyclic voltammetry of several Pt_xRu_y electrodes in 0.5 M H_2SO_4 with 1.0 M CH_3OH (solid line with open circles) at 25 °C. CH_3OH was introduced into the H_2SO_4 solution while the potential of the Pt_xRu_y electrodes was held at 0.05 V. After an equilibrium time of 5 min, the electrode potential was first scanned in the negative direction until 0.0 V was attained and then scanned in the positive direction. The first positive potential scan is shown. The CV recorded in a methanol-free 0.5 M H_2SO_4 solution is also shown for comparison (solid line with shading). Scan rate is 0.01 V s^{-1}. (B) Plot of methanol decomposition charge density during the first positive potential scan as a function of Ru composition.

decomposition can occur. Anodic current corresponding to methanol decomposition begins to flow at 0.1 and proceeds through a maximum at 0.23 V. However, methanol decomposition is not sustained as the current decays to low values at around 0.4 V. This decrease in current is due to the accumulation of chemisorbed partial oxidation products of methanol that block the surface for further methanol adsorption. Notably, Pt is free of surface hydroxides at these potential values, so the oxidation of CO does not occur.

The results of similar measurements for the $Pt_{94}Ru_6$, $Pt_{78}Ru_{22}$, and Pt_0Ru_{100} electrodes are also shown in Figure 3A. The pure Ru electrode shows little difference in current with and without methanol, which reflects a very low adsorption rate for methanol on ruthenium. The electrodes with intermediate Ru content, however, show substantial methanol decomposition currents. The peak and onset potentials for decomposition on the $Pt_{94}Ru_6$ and $Pt_{78}Ru_{22}$ electrodes are 50 mV more negative than that for the $Pt_{100}Ru_0$ electrode. The negative shift in potential is due to an enhancement in the activity of the electrodes for methanol decomposition in the presence of Ru.

Methanol decomposition currents on the $Pt_{94}Ru_6$ and $Pt_{78}Ru_{22}$ electrodes decrease at potentials above 0.2 V. Much like the pure Pt electrode, the formation of adsorbed partial oxidation products on Pt_xRu_y limits further metha-

(47) Gasteiger, H.; Markovic, N.; Ross, P. N.; Cairns, E. J. *Electrochim. Acta* **1994**, *39*, 1825.

nol adsorption. At approximately 0.35 V, the current again begins to increase, indicating that methanol oxidation has commenced. The lack of methanol oxidation before this potential suggests that even though surface hydroxides may be present at the Ru sites at potentials as low as 0.25 V,[48−50] they do not remove the adsorbed species until 0.35 V. These observations support the assertion that the bifunctional mechanism does not play a role until potentials are above 0.35 V. Therefore, the enhancement in the activity in the 0−0.35 V potential region during the first scan is mainly due to an electronic or ligand effect, where the presence of Ru induces a shift in the electronic configuration of Pt such that the decomposition of methanol is enhanced.[3,17,47,51]

Figure 3B shows the total methanol decomposition charge as a function of Ru composition. The charge was determined by integrating the background-subtracted current from Figure 3A between 0.0 and 0.35 V. The decomposition charge increases over pure platinum with the addition of ruthenium. A maximum is observed for electrodes containing 6−25% Ru followed by a decrease in charge at larger Ru contents. The decrease in decomposition charge with increasing Ru content above 25% Ru is due to a decrease in the number of Pt sites available for methanol adsorption. The maximum methanol decomposition current approaches 1.8 times that of pure platinum for the best Pt_xRu_y electrode. Notably, the trend observed in Figure 3B for the composition-dependence of methanol decomposition charge is very similar to the trend in methanol oxidation current in Figure 2B.

Methanol oxidation can occur through a variety of oxidation/dehydrogenation steps. Clearly, electrode deactivation can occur by a reaction pathway involving the formation of carbon monoxide. This is frequently termed the serial reaction pathway.[2]

$$CH_3OH + H_2O \rightarrow CO + H_2O + 4H^+ + 4e^- \rightarrow CO_2 + 6H^+ + 6e^- \quad (2)$$

Alternatively, methanol oxidation can proceed through a parallel pathway involving the formation of weakly bound intermediates, such as formic acid and formaldehyde. Although a variety of parallel reaction pathways can be written, formaldehyde and formic acid appear as partial oxidation products via

$$CH_3OH + H_2O \rightarrow H_2CO + H_2O + 2H^+ + 2e^- \rightarrow HCOOH + 4H^+ + 4e^- \rightarrow CO_2 + 6H^+ + 6e^- \quad (3)$$

Insight into the methanol oxidation pathway can be obtained by performing simultaneous SDEMS measurements. A measure of the complete oxidation reaction is given by the formation of CO_2, which can be detected directly by SDEMS at $m/z = 44$. Formic acid can be detected indirectly at $m/z = 60$ because of the formation of methyl formate:

$$HCOOH + CH_3OH \rightarrow HCOOCH_3 + H_2O \quad (4)$$

Formaldehyde cannot be detected directly but can be calculated by a material balance (vide infra).

Simultaneous electrochemical and SDEMS measurements were performed on the Pt_xRu_y electrodes during scanned and stepped potential measurements to elucidate the dominant reaction products. A typical result for a combined cyclic voltammetry (CV) and mass spectrum cyclic voltammetry (MSCV) experiment is shown in Figure 4 for the $Pt_{94}Ru_6$ electrode. This experiment was performed in a manner equivalent to that for the methanol decomposition results in Figure 3. The electrode was held at 0.05 V in 0.5 M H_2SO_4 for several minutes followed by the addition of 1.0 M CH_3OH. After an additional 5 min at 0.05 V, the electrode potential was scanned to 0.0 V and then in the positive direction to 0.9 V. The electrode current was simultaneously measured along with mass signals at $m/z = 44$ and 60 using a capillary inlet probe positioned directly above the electrode surface at a distance of approximately 100 μm. Additional mass signals, including $m/z = 2$ and 75, were also measured during these experiments. Hydrogen at $m/z = 2$ was used to deduce electrode separation by periodically scanning into the hydrogen evolution region.[34]

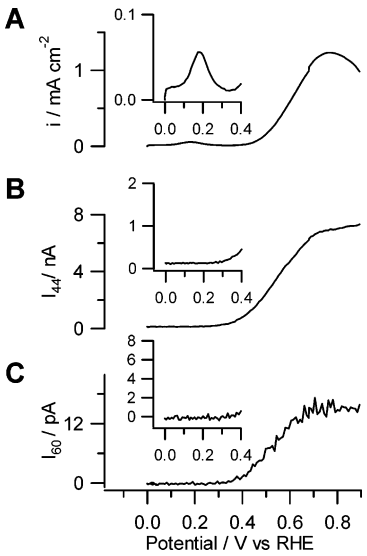

Figure 4. (A) Forward sweep of cyclic voltammogram for $Pt_{94}Ru_6$ electrode and mass spectrometer ion current corresponding to (B) CO_2 ($m/z = 44$) and (C) $HCOOCH_3$ ($m/z = 60$) in a 1.0 M CH_3OH and 0.5 M H_2SO_4 solution at 25 °C. CH_3OH was introduced into the H_2SO_4 solution while the potential of the $Pt_{94}Ru_6$ electrode was held at 0.05 V. After an equilibrium time of 5 min, the electrode potential was first scanned in the negative direction until 0.0 V was attained and then scanned in the positive direction. The first positive potential scan is shown in the figure. Scan rate is 0.01 V s^{-1}. The insets show the magnified 0.0−0.4 V potential region.

The electrochemical current, mass signal for $m/z = 44$, and mass signal for $m/z = 60$ are shown for $Pt_{94}Ru_6$ in Figure 4. The insets depict a magnified version of the data in the low potential region where methanol decomposition occurs. The electrochemical current (Figure 4A) shows both methanol decomposition (inset) and methanol oxidation as the potential is scanned in the positive direction. The small peak in the UPD-H region (Figure 4A, inset) reflects methanol decomposition. Notably, measurements of CO_2 (Figure 4B, inset) and methyl formate (Figure 4C, inset) are featureless in this potential region. A similar observation was made in a prior DEMS study.[51,52] The absence of CO_2 ion current in the UPD-H potential region suggests that little, if any, CO_2 is formed between 0 and 0.35 V. The decomposition process primarily results in the formation of a strongly bound, partial oxidation product. In addition, the absence of methyl

(48) Hadzi-Jordanov, S.; Angerstein-Kozlowska, H.; Vukovic, M.; Conway, B. E. *J. Phys. Chem.* **1977**, *81*, 2271.
(49) Green, C. L.; Kucernak, A. *J. Phys. Chem. B* **2002**, *106*, 1036.
(50) Green, C. L.; Kucernak, A. *J. Phys. Chem. B* **2002**, *106*, 11446.
(51) Krausa, M.; Vielstich, W. *J. Electroanal. Chem.* **1994**, *379*, 307.
(52) Vielstich, W.; Xia, X. H. *J. Phys. Chem.* **1995**, *99*, 10421.

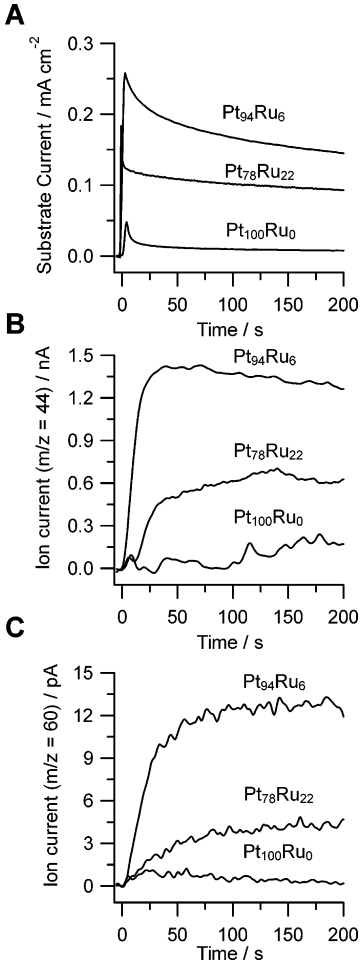

Figure 5. (A) Pt_xRu_y electrode current densities, (B) ion currents corresponding to CO_2 ($m/z = 44$), and (C) $HCOOCH_3$ ($m/z = 60$) versus time after stepping the substrate electrode potential from 0.05 to 0.550 V (vs RHE) in a solution containing 1.0 M CH_3OH and 0.5 M H_2SO_4 at 25 °C. The results for $Pt_{100}Ru_0$, $Pt_{94}Ru_6$, and $Pt_{78}Ru_{22}$ electrodes are shown.

formate ion current indicates that formic acid is not formed during methanol decomposition or is formed in very small quantities. The most likely product of methanol decomposition in this potential region is adsorbed carbon monoxide, although formaldehyde cannot be ruled out. This is consistent with prior electrochemical measurements where methanol decomposition experiments were followed by electrochemical stripping, which demonstrated the presence of adsorbed CO following decomposition.[7,9,10]

At potentials greater than 0.35 V, carbon dioxide and methyl formate are both detected at the $Pt_{94}Ru_6$ electrode. The appearance of these products coincides with the increased substrate current at these potential values and reflects both the complete and partial oxidation of methanol under these conditions. In a qualitative sense, the ion current for CO_2 and $HCOOCH_3$ follow a trend that is similar to the electrochemical current between 0.35 and 0.9 V.

To assess the activity of the Pt_xRu_y electrodes, electrochemical and SDEMS measurements were performed at different potential values. Figure 5A depicts electrochemical and ion current transients corresponding to the electrodes containing 0%, 6%, and 22% Ru, following a step in potential from 0.05 to 0.55 V. The current is recorded for a period of 5 min.[53] For each electrode, the electrochemical current increases initially and then decays to a lower value over a period of time. This decay is the result of electrode deactivation, which is presumably due to the accumulation of adsorbed partial oxidation products formed during methanol oxidation.[54,55] A comparison of the $Pt_{100}Ru_0$, $Pt_{94}Ru_6$, and $Pt_{78}Ru_{22}$ electrodes shows that the Ru-containing electrodes exhibit substantially larger methanol oxidation current densities at 0.55 V.

Parts B and C of Figure 5 show the CO_2 and $HCOOCH_3$ ion currents at $m/z = 44$ and $m/z = 60$ recorded as a function of time at 0.55 V for electrodes containing 0%, 6%, and 22% Ru. Following the potential step, the CO_2 and the $HCOOCH_3$ ion currents initially increase and then reach a plateau value after a period of time. The CO_2 ion current reaches the plateau more quickly than the $HCOOCH_3$ ion current. The lag in $HCOOCH_3$ ion current is partly related to the lower diffusion coefficient of $HCOOCH_3$ in solution compared to CO_2 and also to the finite rate of its formation due to the reaction between formic acid and methanol. Considerably higher CO_2 and $HCOOCH_3$ ion currents are detected for the Ru-containing electrodes compared to the $Pt_{100}Ru_0$ electrode at this potential. The data clearly indicate that CO_2 and HCOOH (as seen by $HCOOCH_3$) are formed simultaneously during the oxidation of methanol at the platinum and the codeposited Pt_xRu_y electrodes.

The CO_2 and $HCOOCH_3$ signals can be used to quantify the current efficiency and the product distribution during methanol oxidation.[42,43,56] In particular, the CO_2 current efficiency, which reflects the number of moles of CO_2 produced per mole of methanol reacted, can be determined by comparing the CO_2 ion current to the electrochemical current. With a proper calibration of the CO_2 ion signal (i_{44}), the instantaneous efficiency (ϵ) of the complete oxidation reaction can be determined by comparing it to the electrochemical current (i_f) according to eq 5.[43,56]

$$\epsilon = \text{CO}_2 \text{ current efficiency} = \frac{\text{moles of CO}_2 \text{ produced}}{\text{moles of CH}_3\text{OH reacted}} = \frac{i_{44}/k_{44}}{i_f/6} \quad (5)$$

The constant k_{44} relates the CO_2 ion current to the equivalent moles of CO_2 detected at the mass spectrometer inlet. It is determined by measuring the CO_2 ion current during oxidation of a monolayer of adsorbed CO on platinum. The ion current is compared to the equivalent number of moles of CO_2 produced during this reaction, which is given by the electrochemical current. Similarly, the ratio of total charge can be used.[43,56]

$$k_{44} = \frac{i_{44}}{i_f/2} = \frac{Q_{44}}{Q_f/2} \quad (6)$$

A typical value for this constant is 5.7×10^{-5} in units of (ion charge)/(electrochemical charge). Notably, this number is influenced by the separation distance between the electrode surface and the capillary inlet in the SDEMS configuration as well as by the inner diameter of the capillary. Care was taken to perform all measurements at a constant separation of approximately 100 μm with a single capillary diameter. The separation was verified by measuring the ion current for hydrogen evolution at a

(53) Iwasita, T.; Hoster, H.; John-Anacker, A.; Lin, W. F.; Vielstich, W. *Langmuir* **2000**, *16*, 522.

(54) Herrero, E.; Franaszczuk, K.; Wieckowski, A. *J. Phys. Chem.* **1994**, *98*, 5074.

(55) Lu, G. Q.; Chrzanowski, W.; Wieckowski, A. *J. Phys. Chem. B* **2000**, *104*, 5566.

(56) Wang, H.; Loffler, T.; Baltruschat, H. *J. Appl. Electrochem.* **2001**, *31*, 759.

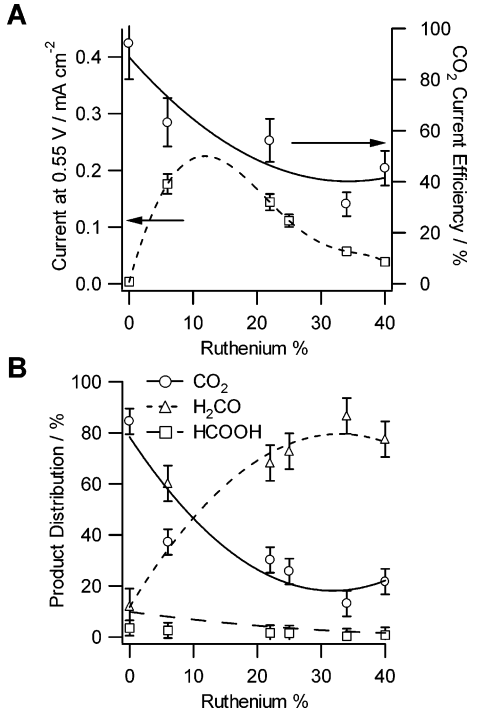

Figure 6. (A) Pt_xRu_y electrode current densities and CO_2 current efficiencies recorded 5 min after a potential step from 0.05 to 0.55 V in a 1.0 M CH_3OH and 0.5 M H_2SO_4 solution as a function of Ru composition. (B) Product distribution calculated at 5 min after a potential step from 0.05 to 0.55 V as a function Ru composition.

fixed electrode current and setting the tip position at a value to keep this current constant in the various experiments.[34]

A current efficiency of 100% indicates that complete oxidation of methanol is achieved and all of the electrochemical current is accounted for by detected CO_2 product. An efficiency of less than 100% indicates that fewer than six electrons are being collected per reacted molecule, which can only occur by partial oxidation. Presumably, lower efficiencies reflect the formation of products such as formaldehyde and formic acid that are lost from the electrode surface without further oxidation to CO_2.

A number of chronoamperometry experiments were performed at the various Pt_xRu_y electrodes to assess the composition-dependence of the electrode reactivity. Figure 6 shows the substrate current and instantaneous current efficiency (Figure 6A) along with the product distribution (Figure 6B) as a function of Ru content. The results all correspond to experiments where data was recorded 5 min after the electrode potential was stepped from 0.05 to 0.55 V. The electrochemical current shows a variation in activity with Ru content. The addition of Ru increases the current compared to pure Pt. The electrodes with compositions $Pt_{94}Ru_6$ and $Pt_{78}Ru_{22}$ exhibit the greatest current density, while the pure Pt and higher-Ru-containing electrodes are less active. Although the $Pt_{94}Ru_6$ electrode shows the highest current, a fit of the data to a continuous curve suggests that the optimum lies in a range of compositions between 5 and 30% Ru with a maximum near ~10%. This is consistent with the cyclic voltammetry results from Figure 2B and with prior measurements on electrochemically deposited catalysts.[18,43,53]

Current efficiencies for the various Pt_xRu_y electrodes are determined by using the measured electrochemical and CO_2 ion current in combination with eqs 5 and 6. The pure Pt electrode shows the highest efficiency. Greater than 90% of the methanol that is oxidized is converted to CO_2. Notably, this number is potential-dependent. Indeed, previous work indicates that lower efficiencies are observed at lower applied potentials and in the oxide region.[46] The trend in efficiency at 0.55 V shows that the value drops as the Ru content increases. The most active compositions, which are electrodes $Pt_{94}Ru_6$ and $Pt_{78}Ru_{22}$, show efficiencies near 60%, while the higher-Ru-containing electrodes have efficiencies that drop to only 40%. These data reflect the loss of methanol to partial oxidation products, which increases with increasing Ru content.

The product distribution can be determined by considering the carbon dioxide and methyl formate ion currents along with the electrochemical oxidation current.[42,43,56] If we assume that formaldehyde, formic acid, and carbon dioxide are the only soluble products formed by methanol oxidation, the oxidation current (i_{CH_3OH}) can be divided into contributions for each of these products.

$$i_{CH_3OH} = i_{H_2CO} + i_{HCOOH} + i_{CO_2} \tag{7}$$

The CO_2 current (i_{CO_2}) is determined by

$$i_{CO_2} = 6(i_{44}/k_{44}) \tag{8}$$

where i_{44} is the ion current and k_{44} is the conversion factor given by eq 6. The HCOOH current (i_{HCOOH}) is determined by a similar equation,

$$i_{HCOOH} = 4(i_{60}/k_{60}) \tag{9}$$

where i_{60} is the methyl formate ion current and k_{60} is the conversion factor relating the methyl formate ion current to the electrochemical current for formic acid formation. This value was estimated to be 9.0×10^{-6} in units of (amps of ion current)/(amps of faradaic current). The H_2CO current can then be found by solving eq 7 for i_{H_2CO}. The total moles of product can then be represented by the sum of these currents divided by the appropriate stoichiometric factors.

$$n_{total} = i_{H_2CO}/2 + i_{HCOOH}/4 + i_{CO_2}/6 \tag{10}$$

The mole fraction of formaldehyde can then be calculated by the ratio

$$x_{H_2CO} = \frac{n_{H_2CO}}{n_{total}} = \frac{i_{H_2CO}/2}{i_{H_2CO}/2 + i_{HCOOH}/4 + i_{CO_2}/6} \tag{11}$$

Similar equations can be written for formic acid and carbon dioxide. Although the formaldehyde can, in principle, be directly measured through the signal corresponding to dimethoxymethane at $m/z = 75$,[6] the sensitivity is too low to give an accurate estimate at methanol concentrations of 1 M or below (vide supra).

A summary of the product distribution results is given in Figure 6B as a function of Ru content following a potential step from 0.05 to 0.55 V. At each electrode composition, the total amount of H_2CO, HCOOH, and CO_2 sums to 100%. The pure Pt electrode ($Pt_{100}Ru_0$) exhibits a high conversion of methanol to carbon dioxide. Nearly 85% of the product is CO_2, while the remainder is H_2CO and HCOOH. As the ruthenium content increases, the fraction of CO_2 formed decreases as does that corresponding to formic acid. However, the formaldehyde fraction steadily increases with increasing Ru content. As the Ru content exceeds 15%, formaldehyde becomes the dominant

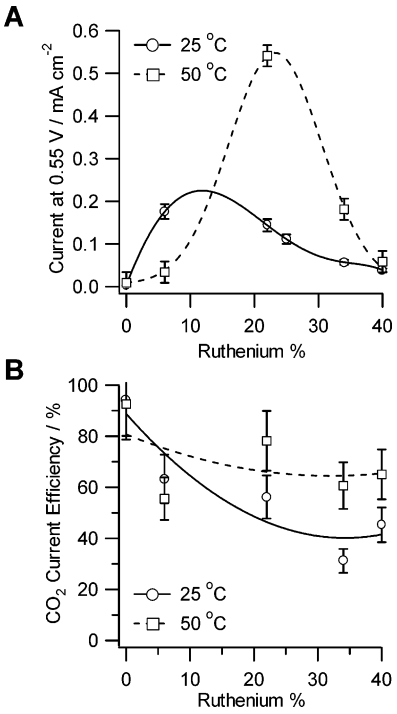

Figure 7. (A) Pt_xRu_y electrode current densities recorded 5 min after a potential step from 0.05 to 0.55 V in a 1.0 M CH_3OH and 0.5 M H_2SO_4 solution at 25 °C (open circles) and 50 °C (open squares), as a function of Ru composition. (B) CO_2 current efficiencies calculated at 5 min after a potential step from 0.05 to 0.55 V as a function Ru composition at 25 and 50 °C.

oxidation product. At 50% Ru, formaldehyde accounts for almost 80% of the product, carbon dioxide accounts for around 20% of the product, and the formic acid fraction is near zero. These results clearly indicate that, at least for the potential values considered here, complete oxidation decreases with increasing Ru content as the partial oxidation path involving the formation of formaldehyde dominates.

Initial experiments examining the reactivity of these Pt_xRu_y catalysts at higher temperatures are illustrated in Figure 7. These results compare electrochemical and mass spectrometry measurements taken at temperatures of 25 and 50 °C following a 5 min potential step from 0.05 to 0.55 V. Electrochemical current densities are shown in Figure 7A, while results of SDEMS current efficiency measurements are shown in Figure 7B.

At 25 °C the trend in current density with catalyst composition shows a maximum in the range 5−25% Ru, with the highest value measured for the $Pt_{94}Ru_6$ composition. At 50 °C, the current density has increased for many of the electrodes, and the highest value is almost 3 times greater than that observed at 25 °C. In addition, the maximum activity is now seen in a higher-Ru-content composition range between 15% and 35% Ru. The highest measured current corresponds to the $Pt_{78}Ru_{22}$ electrode, while the $Pt_{94}Ru_6$ electrode exhibits one of the lowest current values. The higher-Ru-content electrodes are now also showing activity that was not seen at the lower temperature.

This change in activity can be explained in terms of the enhanced activity afforded by the higher temperature as well as the change in behavior of the catalyst materials. At 25 °C, the Ru sites are incapable of adsorbing and decomposing methanol, which favors higher activity in the lower-Ru-content electrodes. As the temperature is increased, the ability of Ru sites to adsorb and decompose methanol improves, which results in improved performance for higher-Ru-content electrodes.[57]

The current efficiencies plotted in Figure 7B also depict a change in behavior at higher temperatures. At 25 °C, the $Pt_{100}Ru_0$ electrode exhibited the greatest conversion of methanol to carbon dioxide at over 90%. The same is true at 50 °C. However, the drop in efficiency at higher Ru content that is observed at 25 °C is not as significant as the temperature is increased. The higher-Ru-content electrodes exhibit efficiencies that hover between 60% and 80% at 50 °C as opposed to the range 40−60% seen at 25 °C. These data indicate that a larger fraction of methanol is oxidized completely to carbon dioxide at higher temperature at the expense of the partial oxidation products seen at 25 °C.

Conclusions

This work used a combination of electrochemical and scanning differential electrochemical mass spectrometry to characterize methanol oxidation on a series of electrodeposited Pt_xRu_y band electrodes. Both cyclic and stepped potential measurements depict a composition-dependent activity with a maximum current density in the range 5−30% Ru at 25 °C. These results are consistent with the maximum activity observed for arc-melted Pt−Ru alloys,[17,57] electrodeposited Ru on Pt,[53] and "spontaneously deposited" Ru on Pt.[18] Methanol adsorption measurements indicate that Ru does not adsorb and decompose methanol. However, the Pt_xRu_y electrodes show a composition-dependent methanol decomposition behavior that is consistent with the oxidation current, which suggests that methanol decomposition is the rate-determining step at 25 °C. SDEMS was used to determine the current efficiency and the product distribution for methanol oxidation. These measurements indicate that the complete oxidation pathway is favored for pure Pt but decreases with increasing Ru content and that formaldehyde is the major partial oxidation product. Increasing the system temperature to 50 °C shifted the maximum activity to higher Ru compositions and increased the current efficiency. This behavior reflects more complete methanol oxidation at higher temperatures and suggests that the reaction mechanism is evolving as the temperature increases.

Ultimately, this work demonstrates the utility of combined electrochemical and mass spectrometry measurements to elucidate information about both the activity and the reaction pathway of methanol oxidation as a function of catalyst composition and temperature. These measurements illustrate the ability to characterize a number of electrodes in a combinatorial fashion using multi-electrode voltammetry and scanning mass spectrometry characterization. This allows one to rapidly and efficiently evaluate catalytic activity and ensure consistent and uniform conditions during analysis.

Acknowledgment. The authors thank the Office of Naval Research (Grant ONR N00014-00-1-0494), the National Science Foundation (Grant CTS 9875496), and the Donors of the Petroleum Research Fund, as administered by the American Chemical Society, for partial support of this research. We also thank Catherine Dukes of the University of Virginia Surface Science Laboratory for assisting with AES measurements.

LA035567I

(57) Gasteiger, H. A.; Markovic, N.; Ross, P. N.; Cairns, E. J. *J. Electrochem. Soc.* **1994**, *141*, 1795.